Gestation and lactation exposure to nicotine induces transient postnatal changes in lung alveolar development

Sanja Blaskovic[1,2*], Yves Donati[1,2*], Filippo Zanetti [1, 2], Isabelle Ruchonnet-Metrailler[1,2], Sylvain Lemeille[2], Tiziana P. Cremona[3], Johannes C. Schittny[4], Constance Barazzone-Argiroffo[1,2]

[1]Department of Pediatrics, Gynecology and Obstetrics, Faculty of medicine; Geneva, Switzerland; [2]Department of Pathology and Immunology, Faculty of medicine, University of Geneva, Switzerland; [3]Harward School of Public Health; [4]Institute of Anatomy, University of Bern, Switzerland

*Equal contribution

Abbreviated title:

Alveolar development in mice: does nicotine interfere?

Keywords: nicotine, lung development, alveolarization, developmental kinetics

Corresponding author:

Constance Barazzone-Argiroffo

Department of Pediatrics, Gynecology and Obstetrics

4 rue Gabrielle-Perret-Gentil

CH - 1211 Genève 14

Constance.Barazzone@hcuge.ch

ABSTRACT

Harmful consequences of cigarette smoke (CS) exposure during lung development can already manifest in infancy. In particular, early life exposure to nicotine, the main component of CS, was shown to affect lung development in animal models. We aimed to characterize the effect of nicotine on alveoli formation. We analyzed the kinetics of normal alveolar development during the alveolarization phase and then looked at the effect of nicotine in a mouse model of gestational and early life exposure. Immunohistochemical staining revealed that the wave of cell proliferation (i.e. vascular endothelial cells, alveolar epithelial cells (AEC) type II and mesenchymal cell) occurs at pnd8 in control and nicotine-exposed lungs. However, FACS analysis of individual epithelial alveolar cells revealed nicotine-induced transient increase of AEC type I proliferation and decrease of vascular endothelial cell proliferation at pnd8. Furthermore, nicotine increased the percentage of endothelial cells at pnd2. Transcriptomic data also showed significant changes in nicotine samples compared to the controls on cell cycle associated genes at pnd2, but not anymore at pnd16. Accordingly, the expression of survivin, involved in cell cycle regulation, also follows a different kinetics in nicotine lung extracts. These changes resulted in an increased lung size detected by stereology at pnd16, but no longer in adult age, suggesting that nicotine can act on the pace of lung maturation. Taken together, our results indicate that early life nicotine exposure could be harmful to alveolar development independently from other toxicants contained in CS.

INTRODUCTION

During fetal development, lungs undergo several orchestrated steps to ensure adequate gas exchange. The successive embryonic, pseudoglandular, canalicular, saccular and alveolar phases are required to achieve functionality of the various parts of the lung, such as the conducting airways or respiratory units formed by alveoli (21, 53). Both genetic and environmental factors can influence lung development (18). The consequences of harmful events can manifest at birth, but also later in life. Exposure to cigarette smoke (CS) during early life has been widely associated with wheezing in childhood, and later in life with the development of chronic metabolic or cardiovascular diseases, such as diabetes or hypertension (5, 18), or chronic obstructive pulmonary disease (COPD) (10, 46, 47). Nicotine, one of the main components of CS, can freely cross the placenta and may harm the developing fetus (17). Nicotine exposure during pregnancy and lactation has been studied in rats and monkeys where it reduces gas exchange surface (39, 55). Furthermore, increased airway length and no change in the alveolar intercepts in mice exposed to nicotine were detected (58, 60). Finally, accelerated development of the bronchiolar tree was described in lambs (51). Most of the effects described worsened when pups were exposed to nicotine during the prenatal and postnatal period (10). In humans, there is no evidence that nicotine replacement therapy (NRT) induces major congenital abnormalities (8) and very few information is available on e-cigarette use during pregnancy (59). Since the effect of nicotine on alveolar development and in particular on the dynamics of cell death and proliferation has been poorly studied, we aim to better characterize a) the dynamics of different cell types during lung alveolarization, and b) the effect of *in utero* and lactation exposure to nicotine on the development of alveoli. Mice are born at the end of the saccular phase of lung

development, and therefore the process of alveolarization occurs after birth and is easier to study than in other animal species.

To address our questions we exposed mice to nicotine during gestation and lactation to mimic pre- and postnatal exposure, and assessed lungs at post-natal day (pnd) 2 (end of saccular phase), 8 (early alveolar phase) and 16 (middle alveolar phase). Our results indicate dynamic processes of proliferation, with a peak detected at pnd8 and caused by three cell types: vascular endothelial cells, mature AEC type II and mesenchymal cells. Nicotine had no effect on proliferation dynamics when measured in the whole lung. Instead, we observed an effect on individual cell proliferation levels of endothelial cells and AEC type I cells that was accompanied by extensive genetic changes detected at the beginning of alveolar phase. Nicotine also increased lung and parenchyma volume and septal surface area at pnd16. The study of the cell cycle strongly suggest an acceleration in lung maturation. Majority of nicotine-induced changes were lost by pnd16, indicating that these effects are transient, except for the bigger lung volume detected at pnd16, that was no longer present in adult age.

LIST OF ABBREVIATIONS

AEC	alveolar epithelial cell
AQP5	Aquaporin 5
COPD	chronic obstructive pulmonary disease
CS	cigarette smoke
Csf3	Granulocyte colony stimulating factor 3
Dlx5	distal-less homebox 5
Dmp1	cyclin D binding myb-like protein
ECM	extracellular matrix
FACS	Fluorescence-activated cell sorting
Fgf23	Fibroblast growth factor 23
Hox	Homebox gene
HRP	Horseradish peroxidase
Igf1	Insulin like growth factor 1
Il	interleukin
Irg1	Immune-responsive gene 1
Ltbp4	Latent Transforming Growth Factor Beta Binding Protein 4
MHCII	major histocompatibility complex class II
MLI	mean linear intercept
Nrp1	Neuropilin 1
Orm	Orosomucoid
PBS	phosphate buffered saline
PCNA	proliferating cell nuclear antigen

102	*Pdgf-a*	Platelet Derived Growth Factor Subunit A
103	PDPN	Podoplanin
104	Pnd	post-natal day
105	RML	right middle lobe
106	RT	room temperature
107	*Serpina*	Serpin Peptidase Inhibitor Clade A gene
108	SPC	surfactant protein C
109	TUNEL	terminal deoxynucleotidyltransferase–mediated dUTP nick end
110		labeling

MATERIALS AND METHODS

Animals

The animal procedures were performed in accordance with the Institutional Ethics Committee on Animal Care (Geneva, Switzerland) and the Cantonal Veterinary Office (authorization number GE/32/15 and GE/62/14). C57BL/6J mice (*Mus Musculus*) obtained from the animal facility of University of Geneva were kept under specific-pathogen-free conditions. Housing conditions were 12 hours day and 12 hours night. Mice had access to food and drinking water ad libitum. Nicotine (200 mg L^{-1}) was started immediately after mating and administered to the females in drinking water supplemented with 2% saccharin for the whole period of gestation and lactation (nicotine group). Exposure to nicotine was determined by measurements of cotinine (measurements were done according to manufacturer protocol of ELISA kit, #501.301, Immunalysis, USA), the main metabolic product of nicotine, in the serum of the mothers and pups upon sacrifice at pnd 2-16. The values obtained for the mothers were 130 ± 88 ng/ml (n=8) and for the pups 70.6 ± 31 ng/ml (n=40), corresponding to values of medium to heavy smoker (36). There was no statistical difference in cotinine values measured at different pnd. As a control, we used drinking water with 2% saccharin (control group). Pups were sacrificed at pnd2, 8 and 16 with Esconarkon (150 mg/kg, Streuli Pharma SA, Uznach) and lungs subjected to subsequent analysis. The litter size varied from 2-11 pups, and we did not normalize for it in our experiments. The sex of the pups was determined by testing for the expression of sycp3-like y-linked and X-linked lymphocyte-regulated complex genes via PCR (29). Furthermore, female and male pups were analyzed together as one group as our preliminary experiments and literature suggests no effect of sex on lung development (40). Pups were not weaned at different pnd analyzed as they are normally weaned at pnd21.

Lung Instillation procedure was performed as described previously (34). Briefly, the airspace of the lung was filled with solution of 4% paraformaldehyde in phosphate buffered saline (10 mM sodium phosphate, containing 127 mM sodium chloride, pH 7.4) at a constant pressure of 20 cm water column. At this pressure, the lung reaches roughly its total lung capacity (49).

Stereological analysis

Lung volume was determined by applying the water displacement method (52). Five µm thick paraffin sections of the embedded right middle lobe (RML) lobes were cut along the longitudinal axis. Equally distributed sections obtained at 7 to 9 positions (depending on lung size) were dried overnight at 37˚C and stained with hematoxylin and eosin (26). Eighty to 100 images per RML (i.e. per animal) were acquired using a Leica DM RB light microscope (Glattbrugg, Switzerland) equipped with a motorized Maerzheuser XY stage (Wetzlar, Germany). N PLAN 20x/0.40 PH 1 (Leica P/N 506024) objective was used. Images were taken with the ColorView IIIu 5 MegaPixel CCD Color Camera (Olympus, Münster, Germany) provided by microscopy imaging center core facility at the University of Bern. Finally, 40 images per animal were selected using a systematic random sampling scheme (4).

All the measurements were performed on lung RML. The volume of the RML, volume of the lung parenchyma and septa, septal surface area density and absolute septal surface area were estimated/calculated as described previously in (34).

Gene expression

Offspring lungs were collected at pnd2 and 16, snap frozen in liquid nitrogen and stored at -80˚C. RNA was isolated and purified using Macherey-Nagel purification kit (Germany). Six and five offspring lungs were used for pnd2 and 16 in control group and five and three offspring lungs were used for pnd2 and 16 in the nicotine group. cDNA libraries were constructed by the Genomic platform of the University of Geneva using the Illumina TruSeq RNA Sample Preparation Kit (CA, USA) according to the manufacturer's protocol. Libraries were sequenced using single-end (50nt-long) on Illumina HiSeq2500. FastQ reads were mapped to the ENSEMBL reference genome (GRCm38.80) using STAR version 2.4.0j (9) with standard settings, except that any reads mapping to more than one location in the genome (ambiguous reads) were discarded (m = 1). A unique gene model was used to quantify reads per gene. Briefly, the model considers all annotated exons of all annotated protein coding isoforms of a gene to create a unique gene where the genomic region of all exons are considered coming from the same RNA molecule and merged together. All reads overlapping the exons of each unique gene model were reported using feature Counts version 1.4.6-p1 (42). Gene expressions were reported as raw counts and in parallel normalized in RPKM in order to filter out genes with low expression value (1 RPKM) before calling for differentially expressed genes. Library size normalizations and differential gene expression calculations were performed using the package edgeR (48) designed for the R software (43). Only genes having a significant fold-change (Benjamini-Hochberg corrected p-value < 0.05) were considered for the rest of the RNAseq analysis. MDS plot was obtained with the package edgeR designed for R. Distances on the Multidimensional scaling plot represent the expression differences between samples (based on fold changes between samples). Data analysis was performed using MetaCore software (https://portal.genego.com/). Complete results of RNAseq analysis are deposited in Gene

178 Expression Omnibus (GEO) repository under the following link
179 http://www.ncbi.nlm.nih.gov/geo/query/acc.cgi?acc=GSE102239.
180
181 *Immunohistochemistry staining*

182 Paraffin-embedded or cryosections of mouse lungs, collected at pnd2, 8 and 16, were stained
183 according to the cell signaling technology standard protocol (https://www.cellsignal.com/).
184 Briefly, paraffin-embedded samples were deparaffinized using xylene and 95-100% ethanol and
185 subsequently hydrated in H_2O. We applied the following antigen retrieval methods for single
186 epitope staining: heat-induced epitope retrieval for 10 min in 0.01 mol/L citrate buffer (pH 6.0)
187 for prosurfactant protein C (SPC) antigen and pressure-induced epitope retrieval (20 Bar) in 0.01
188 mol/L citrate buffer (pH 6.0) for Ki67. Endogenous peroxidases were blocked with DAKO
189 peroxidase block solution. Both primary and secondary antibodies were diluted with DAKO
190 antibody diluent. We applied the primary antibodies for 1 hour at room temperature (RT).
191 Finally, labelled polymer-HRP anti-rabbit or anti-mouse (Envision + system, DAKO, USA) was
192 used for 30 min at RT and the signal was visualized with diaminobenzidine (DAB, Envision +
193 system) or 3-amino-9-ethylcarbazole (AEC) (Dako SA, Geneva, Switzerland). Sections were
194 counterstained with Hematoxylin (BioGnost, Zagreb). Quantification of positive cells was
195 performed with Definiens software (Germany) provided by bioimaging core facility at the
196 University of Geneva or ImageJ software (U.S. National Institutes of Health). Images were taken
197 with Axio scan.Z1 (Carl Zeiss, Germany). Quantification of positive cells was performed with
198 Definiens software (Germany) provided by bioimaging core facility at the University of Geneva
199 or ImageJ software.

Cryosections were fixed for 15 minutes (min) at RT in 4% paraformaldehyde (PFA), and subsequently washed 3 times for 5 min in PBS. The samples were further incubated in the blocking solutions (5% normal goat serum + 0.3% triton X-100 in PBS) for 1 hour at RT, and then exposed to primary antibodies (PDPN and CD31) diluted in the blocking solution for 1 hour at RT. Sections were than washed with PBS (3x5 min) and exposed to fluorochrome coupled secondary antibodies again for 1 hour at RT. The samples were then again washed with PBS and the nuclei were stained with DAPI (5 min at RT) and slides were mounted with FluorSave™ reagent (Millipore). Images were acquired with Zeiss LSM800 confocal microscope with Apochromat objective 63x/N.A. 1.4 oil immersion and further processed by Imaris (https://imaris.oxinst.com/) and Huygens (HuygensSoftware) software. For all the information about the primary and secondary antibodies see the section "antibodies and reagents" in the supplemental material.

Measure of cell death

For paraffin sections of fixed lung, terminal deoxynucleotidyltransferase–mediated dUTP nick end labeling (TUNEL) was performed with an *in situ* apoptosis detection kit according to the protocol of the manufacturer (ApopTag®, Chemicon, Temecula, CA). Briefly, 5 µm thick paraffin sections were deparaffinized and then treated with proteinase K (ROCHE, 20 µg/ml 30min 37°C) to unmask DNA. The mix containing TdT enzyme and Dig-labelled dNTP in a reaction buffer is added to the sections and allowed to react for 1h at 37°C with the free DNA resulting from strand breaks or fragmentation. dNTP tail is revealed using a horse radish peroxidase (HRP)-coupled anti-DIG antibody and AEC substrate. Sections were counterstained with Hematoxylin (BioGnost, Zagreb). As reported in Immunohistochemistry staining section,

222 Images were taken with Axio scan.Z1 and quantification of positive cells was performed with
223 Definiens software.

224 *Western blot analysis*

225 Cells were lysed with the following buffer: TRIS 50 mM, NaCl 250 mM, Triton X-100 1%,
226 Sodium Deoxycholate 0.5%, SDS 0.1%, pH 8.0. Total protein extract was quantified by means
227 of a bicinchoninic acid protein assay reaction kit (Pierce, Rockford, IL, USA) and 40 μg were
228 separated on 10, 12 or 15% SDS-PAGE (depending of the targeted protein size) and
229 subsequently transferred to a nitrocellulose membrane. The membranes were blocked for 15-30
230 min at room temperature (RT) in a blocking buffer (phosphate buffered saline (PBS), 0.1%
231 Tween 20, 5% bovine serum albumin). Incubation with primary antibodies was performed
232 overnight, at 4^0C and incubation with secondary antibodies was performed at RT for 1h. Proteins
233 were revealed with chemiluminescence reagents (ProtoGlow ECL, National Diagnostics, USA).
234 Images were quantified using ImageJ software.

235 *FACS analysis of cell cycle*

236 Tissue digestion and isolation of cells from control and nicotine-exposed mouse lungs for FACS
237 analysis was performed as described in Donati et al. (the full technical description is available in
238 the adjacent manuscript). The cells were always used fresh and analyzed by FACS at separate
239 times corresponding to harvest. We used CD31 to mark the endothelial cells and CD326 for the
240 epithelial cells. As described in the adjacent manuscript (method section), with the lung digestion
241 protocol we limited the contamination of bronchial cells, and further focused only on alveolar
242 cells by using markers that stain alveolar cells. To distinguish between type I and II epithelial

cells, we used podoplanin (PDPN) and major histocompatibility complex class II (MHCII) as described in Donati et al. (see antibodies section in supplementary information). All the analysis was performed in CD45 negative ($CD45^{neg}$) population, to exclude blood-derived cells. The cell cycle analysis technique was adapted from Darzynkiewicz et al. (7). Briefly, $4x10^6$ labelled cells were washed with PBS and fixed in PBS-0.5% formaldehyde for 15min. the fixative solution was removed by centrifugation, and the cell pellet was resuspended for 30min on ice in 1ml PBS, 1% BSA, and 0.1% saponin containing 2ug/ml of Hoechst33342. After washing, cells were kept on ice until flow cytometer processing in 0.5ml PBS, 1% BSA containing 2ug/ml Hoechst33342. Analysis events were recorded on a BD LSR Fortessa and data were analyzed with FlowJo software (Version 10.5.0).

Statistical analysis

Results were expressed as mean ± standard deviation (sd), except for supplementary Figure 1 (mean ± s.e.m.), and were analyzed in PRISM by either a) 2-way ANOVA multiple t-test analysis with recommended tukey or sidak correction for determining significance between control and nicotine-treated samples at different days or b) nested 1-way ANOVA with tukey correction for determining significance within the control samples at different days. The threshold for the significance was set at $p \leq 0.05$. Any analysis that differs from these described above is noted in the individual figure legend.

RESULTS

In utero exposure to nicotine leads to increased lung size at pnd16

To address whether nicotine exposure *in utero* can affect lung morphology, we performed stereological analysis of lungs collected at three different postnatal days, namely pnd2, pnd8 and pnd16. All the analyses were performed on RML. We first examined the lung volume, parenchyma and septal volume, as well as septal surface area in control mice. All examined parameters increased significantly during normal alveolar development (Table 1). Mean linear intercept (MLI), describing the mean free distance in the air spaces, decreased as expected during alveolar development and significantly between pnd8 and 16 (Table 1). We then analyzed nicotine effect on these parameters. Nicotine increased lung and parenchyma volumes as well as septal surface area, slightly but significantly, at pnd16, but not at pnd2 and 8 (Fig. 1A, B, C and E). Septa volume and MLI values were not affected by nicotine (Fig. 1A, D and F).

Nicotine affects gene profile at pnd2 but not pnd16

In utero exposure to nicotine has been reported to affect gene expression in the brain (24, 56). We examined the whole lungs by RNAseq analysis at the end of saccular phase (pnd2) and then in the middle of alveolar phase (pnd16). Principal component analysis showed a nice segregation between nicotine and the control samples at pnd2, but not anymore at pnd16 (Fig. 2A). At pnd2, we obtained 3957 genes whose mRNA expression was significantly modified by nicotine. Amongst them, 2098 were upregulated and 1859 downregulated in the nicotine group compared to the control. The top 10 most upregulated and downregulated genes upon nicotine exposure are presented in Table 2. The majority of upregulated genes are bone-secreted proteins that do not normally have a lung function and are involved in bone and muscle energy metabolism.

However, some of the genes have been reported to promote lung cancer, such as distal-less homebox 5 (*Dlx5*), or act as tumor suppressors such as cyclin D binding myb-like protein (*Dmp1*) (20, 27). Among the downregulated top 10 genes, the majority are immune system related and some of them are associated with lung-related diseases such as asthma (*Orosomucoid family,* several single nucleotide polymorphisms in ORMDL3 were enriched in asthmatic population)(32), emphysema (*Fgf23,* increased in emphysema and COPD)(23) and COPD (*Csf3,* 1719T single nucleotide polymorphism associated with protection against low lung function in COPD patients)(16). Furthermore, 31% of top 100 downregulated proteins are relevant for lung injury repair (for example, *Il22, Il17f, Irg1, Il1b*) (25, 45, 61). Amongst other nicotine downregulated genes is Serpin Peptidase Inhibitor Clade A (*Serpina*) genes whose deficiency has been associated to severe emphysema (31).

Pathway analysis for data from pnd2 was performed with MetaCore using threshold 1.5 and significance ≤ 0.05. Results for the top 10 upregulated and downregulated pathways is shown in Fig. 2B and C. Top 10 pathways upregulated by nicotine can be sorted into several categories: cell cycle, epithelial to mesenchymal transition, stem cell related pathway, WNT signaling pathway, stromal-epithelial interaction, cell adhesion and DNA damage (Fig. 2B). On the other hand, the top 10 of nicotine downregulated pathways are associated with general immune response or asthma associated immune response (Fig. 2C).

Kinetics of lung cell proliferation and apoptosis during development are not modified by nicotine

First, we addressed the expression of Ki67, normally found only in proliferating cells (Fig. 3A), throughout lung development. We detected a proliferation peak at pnd8. On the other hand,

apoptosis analyzed by TUNEL staining showed no significant difference between analyzed days (Fig. 3B). Neither cell proliferation nor apoptosis was modified by nicotine. Similar results were obtained for the other two proliferation markers: cyclins, in particular cyclin A and D, and proliferating cell nuclear antigen (PCNA) (Fig. S1A-F). As we previously showed that nicotine affects the intrinsic apoptotic pathway in mouse epithelial cells (63), we addressed the expression of BCL and BAX molecules, key players in this pathway, at pnd2, 8 and 16 but again confirmed an absence of effect with nicotine (Fig. S2A and B). To understand the increase in lung volume observed with nicotine at pnd16, we further investigated RNAseq results that were linked to cell proliferation/apoptosis. We focused on cell cycle related genes and genes involved in the WNT pathway upregulated at pnd2 and reported to be crucial in the development of distal lung involved in gas exchange (13, 33). We found a stable expression of β-catenin, the central component of canonical WNT signaling pathway, throughout the three analyzed post-natal days, but detected an upregulation of survivin at pnd8, a downstream target of the β-catenin pathway involved in cell cycle and apoptosis regulation (Fig. 3C and D). The expression of both proteins was affected by nicotine, showing a significant increase at pnd2. This effect was again transient and no longer detected at pnd16 (Fig. 3C and D). The survivin peak detected at pnd8 in the control was not present at any of the analyzed days in nicotine samples, suggesting that survivin expression could follow different kinetics or that the peak, observed at pnd8 in the control, occurred earlier (Fig. 3D).

Nicotine affects proliferation rates of AEC type I and endothelial cells at pnd8 and 16

As some of the effect caused by nicotine might be cell specific and thereby lost in the whole lung population, we analyzed the cell cycle of individual lung cell types by FACS (see explanation of

330 the analysis in Fig. S3). Characterization of lung alveolar populations is described in detailed in
331 Donati and colleagues (see adjacent manuscript). The major proliferating populations were
332 vascular endothelial cells ($CD31^{pos}$), mature AEC type II ($MHCII^{pos}$) and $CD31^{neg}CD326^{neg}$
333 population containing mesenchymal cells, with the highest values of 10.8, 5.4 and 4.8%,
334 respectively, detected at pnd8 (Fig. 4A, B and D), which follow the same trend as the total lung
335 cell populations analyzed by Ki67 (see Fig. 3A). The population of AEC type I
336 ($CD326^{pos}PDPN^{high}$) showed low proliferation rates of 0.6% and 0.7% at pnd2 and 8,
337 respectively, which increased to 1.9% at pnd16 (Fig.4C). Nicotine significantly increased the
338 proliferation rate of AEC type I at pnd8 from 0.7 to 1.6% and also decreased significantly the
339 proliferation rate in endothelial cells at pnd8 and 16 from 10.8 to 9% and 3.65 to 1.4%,
340 respectively (Fig. 4A and C). The proliferative value of AEC type II and $CD31^{neg}CD326^{neg}$
341 population was not affected by nicotine (Fig. 4B and D).
342

343 **Nicotine accelerates early alveolar maturation of AEC type I and II cells**

344 We wished to verify our results on nicotine affected cycling of endothelial and AEC type I cells
345 and analyzed the remaining alveolar population. We therefore stained by IHC mouse lungs at
346 pnd2, 8 and 16 with established alveolar cell type markers, namely PDPN for AEC type I (37),
347 SPC for AEC type II (19) and CD31 for endothelial cells of lung capillaries and vessels (41).
348 Because of their very thin and circle shaped cytoplasm, it is often hard to see the nucleus of
349 endothelial cells of capillaries (Fig. 5B). Furthermore, it was also not easy to adequately match
350 individual nuclei with membranous PDPN staining and therefore quantify the AEC type I cells
351 by IHC (Fig. 5B). We were only able to quantify the SPC staining (Fig. 5A).

352 The density of AEC type II (SPC^{pos}) remained stable throughout all the pnds between 4 and
353 $6x10^4/cm^2$. Nicotine had no effect on the amount of SPC stained cells at any of the days analyzed
354 (Fig. 5A).
355 Determination of percentages of endothelial and AEC type I cells was based on FACS method
356 published by Donati and colleagues (see Materials & Methods section in adjacent manuscript).
357 Furthermore, we used the same approach to address the percentages of other major alveolar cell
358 types, such as Immune ad mesenchymal cells.
359 We found that during development, nicotine caused a significant increase in the number of
360 $CD45^{pos}$ cells, reflecting marginated immune cells (2), and therefore causing a relative decrease
361 in $CD45^{neg}$ cells at pnd2 and 16 (Fig. 6A). The $CD31^{neg}CD326^{neg}$ population, that should contain
362 the mesenchymal cells decreased towards pnd16 and was not affected by nicotine (Fig. 6B and
363 Table 3). We further found a linear increase of vascular endothelial cells during alveolarization,
364 from 7.7% at pnd2 to 15.5% at pnd16 (Fig. 6C and Table 3). At pnd2 nicotine caused an increase
365 in the percentage of endothelial cells compared to control (Fig. 6C). As suggested by Donati and
366 colleagues (see adjacent manuscript), the smaller percentage of AEC type I isolated at pnd8 and
367 pnd16 compared to pnd2 probably reflects lung maturity. Indeed, in a more mature lung AEC
368 type I form cell junctions with the extracellular matrix (ECM) and neighboring cells and
369 isolation of these cells becomes more difficult by FACS. In fact, the highest yield of 8.1% for
370 AEC type I at pnd2 had drastically dropped by pnd16 (Fig. 6D and Table 3). Nicotine induced a
371 significant decrease of the number of extractable AEC type I to 6.2% at pnd2 and 1% at pnd8,
372 suggesting that nicotine accelerates lung maturation (Fig. 6D).
373 As expected the mature type II population, detected by the presence of MCHII, increased
374 significantly during alveolarization from 0.4% at pnd2 to 34.8% at pnd16 (Fig. 6E and Table 3).

375 Here again, we found a significantly higher percentage of mature AEC type II in nicotine-treated
376 lungs at pnd8 (from 18.55 to 25%, Fig. 6E), a finding that goes along with nicotine-induced
377 increase in lung developmental kinetics.

DISCUSSION

Nicotine is one of the main components of CS that affects early lung development (44). Animal studies associated nicotine exposure to decreased airways diameter, enlarged airspace or faster lung development, depending on the time frame and concentration of exposure, and also to the species exposed (51, 60). However, studies looking at alveolarization are rare and controversial (28, 54, 62).

The purpose of this study was a) to analyze the normal alveolar lung development and b) to assess the effect of nicotine exposure during gestation and lactation on the alveolar phase of lung development.

In control mice we observed a cell proliferation peak at pnd8 during lung alveolarization, confirmed by the analysis of three different proliferation markers: Ki67, PCNA, and cyclins (cyclin A and D). Furthermore, levels of survivin, a downstream molecule in the WNT pathway and involved in proliferation, also peaked at pnd8 (57). Levels of apoptosis were constant and low at all analyzed days. The three most abundant proliferating populations, vascular endothelial cells, mature AEC type II and $CD31^{neg}CD326^{neg}$ containing mesenchymal cells, determined by FACS, also showed a cell cycle peak at pnd8. AEC type I showed the lowest level of proliferation, reaching 1.9% at pnd16. These data are in agreement with those published by Yang and colleagues suggesting that AEC type I retain some degree of proliferative potential (62). Because detection of AEC type I by IHC is not accurate, as due to their elongated shape is sometimes hard to match the stained cell with its nuclei, our FACS results are all the more interesting as they enabled specific identification of AEC type I (see adjacent manuscript). Concurrently with lung maturation and extension of the capillary bed during the alveolar phase, vascular endothelial cells and mature AEC type II increased in percentage from pnd2 to pnd16.

401 The percentages of AEC type II were between 5 and $7x10^4/cm^2$ of the lung (Fig. 5A), which is
402 significantly lower than reported for adult rat and human lung (12-16%) (38). As it has been
403 suggested that the alveolar phase lasts until young adulthood, it is probable that the percentage of
404 AEC type II reported at pnd16 was not final and might increase further (54). Finally, we were
405 not able to determine the total amount/percentage of AEC type I due to the limitation of available
406 techniques. The percentage of AEC type I isolated at pnd2 (8.1%) and the corresponding low
407 levels of cell cycling at all measured days suggest that the percentage detected at pnd2 is stable
408 throughout alveolarization. The reported percentages of AEC type I in adult rat or human lung
409 are 8.1% and 8.3% respectively, and are within the range of data described in this manuscript
410 (38). Finally, stereological analysis, reported for RML, nicely reflected lung maturation during
411 alveolar development and showed an increase of both, lung and parenchyma volume, as well as
412 septal surface area from pnd2 to pnd16. On the other hand, mean linear intercept decreased
413 during alveolarization, as expected, due to the process of lung septation. Values for lung RML
414 volume range from 10 µl at pnd2 to 20 and 40 µl at pnd8 and 16, respectively. This is in line
415 with values reported by Yang and colleagues, ranging from 90 to 100 µl for the entire left lung at
416 pnd14 (62). Furthermore, the values obtained for MLI in our study are similar to those published
417 by Pozarska and colleagues (40).

418 We then assessed the effects of nicotine exposure on offspring's lung development.
419 Nicotine is very unstable and is indirectly measured by levels of cotinine, the main metabolic
420 product of nicotine. There is no clear consensus on the levels of cotinine reported for passive
421 smokers; the values vary from study to study and tissue analyzed (saliva, blood or urine). The
422 values range between 5 (measured in saliva) and 30 ng/ml (measured in urine) (12, 14). In our
423 study, the values for cotinine were 130 ± 88 ng/ml, measured in gestant mice and 70.6 ± 31

ng/ml measured in the pups after birth. Based on significantly higher level of cotinine detected in gestant mice, one might expect the highest effect of nicotine at pnd2. However, this trend was confirmed only for the results of RNAseq analysis, where we observed extensive genetic changes induced by nicotine at pnd2 affecting the cell cycle, the canonical WNT pathway, cell adhesion and immune system and for the percentage of endothelial cells. Other parameters, such as percentages of other lung populations and the analysis of their cell cycle obtained by FACS were also affected at later analyzed days. Nevertheless in almost all analyses, the effect of nicotine was no longer present by pnd16, except for the "bigger lung" that was no longer observed in adult mice (Fig. S4). Taken together, these data suggest, that while nicotine induces a variety of changes, these changes are not permanent. Such a transient effect was reported previously, in rats, in the study by Petre et al, where nicotine induced initial decrease in the airspace size immediately after the rats are born, that was followed by a catch-up increase detected in 3 weeks old rats and complete loss of the effect by week 12 after birth (39).

Several results from our FACS analysis hint towards nicotine-induced shift in phase and acceleration of lung maturation, a hypothesis already brought forward by Sandberg and colleagues in 2004 (51), although metabolic pathways have not been addressed in our study. First, we detected a nicotine-induced increase in percentages of vascular endothelial cells at pnd2 and mature AEC type II at pnd8 (Fig. 6C and E). In both cases, the control lung eventually reached the same values by pnd8 and 16 respectively. Second, in spite of nicotine-induced increase in cell cycle detected for AEC type I cells at pnd8, we could isolate lower amount of this cell type at both pnd2 and 8. As explained in Donati et al (see adjacent manuscript), the isolation of AEC type I cells becomes more difficult with aging because a) they undergo extensive structural changes during development, including cell flattening, elongation and

447 folding (62) and b) they develop an increasing number of cell-cell and cell-ECM interactions.
448 We have confirmed this phenomenon in control mice, where after pnd4-5 the percentage of AEC
449 type I isolation drastically drops (data not shown). Therefore, we believe that the lower isolation
450 efficiency of AEC type I at pnd2 and 8 from nicotine-exposed lungs reflects the increased
451 maturation of this lung structure. Third, nicotine-induced increase in lung volume, observed at
452 pnd16, did not persist in adult age. Such transient effect of nicotine on lung volume is consistent
453 with the shift in phase hypothesis. Forth, results from RNAseq analysis at pnd2 showed nicotine-
454 induced upregulation of genes involved in alveolarization, such as genes related to elastin
455 deposition (insulin like growth factor 1 (*Igf1*) and its receptor, *Ltbp4*, fibrilin) and septa
456 formation (*Hox, Pdgf-a, Nrp1*) (3, 11, 15, 22, 30). Finally, two genes involved in different stages
457 of lung development were upregulated in our transcriptomic analysis from nicotine samples at
458 pnd2. IGF1 receptor, whose absence is associated with delayed saccular development (11) and
459 WNT5a related to alveolar development in mice. All these results could support the hypothesis
460 of nicotine-induced lung maturation. Furthermore, ECM proteins such as collagens, known to be
461 involved in cell shape regulation, were also upregulated in nicotine samples. Despite the fact that
462 gene up- or downregulation disappeared at pnd16, changes in lung cell dynamics is of
463 importance in the context of *in utero* and early life programing, leading to increased
464 susceptibility of adults to lung and non-lung diseases, a concept suggested as “fetal origin
465 hypothesis” by Barker and Osmond (1). In line with this, WNT signaling pathway, already
466 shown to be affected by nicotine in various lung cell lines (50, 64, 65) as well as *in vivo* in mice
467 (6) was also reported to be involved in maintaining AEC type II stemness. In particular, Nabhan
468 and colleagues, found that high levels of WNT pathway maintained the progenitors pool while
469 the decrease in WNT lead to transdifferentiation of this pool into a mature AEC type I (35).

Therefore, nicotine effect on alveolar stem cell niche via WNT as well as nicotine-induced transcriptomic changes in genes such as Serpina involved in emphysema and genes related to lung injury might contribute to a higher susceptibility to diseases in adulthood. This hypothesis remains an open question and requires further research. Finally, understanding the impact of nicotine vs CS is required in the context of the increasing interest in CS replacement therapies.

CONCLUSIONS

Our study describes the dynamics of cell cycle and lung alveoli composition during the developmental alveolar phase and identifies three main types of cells responsible for the proliferation peak observed at pnd8, namely vascular endothelial cells, mature AEC type II, and $CD31^{neg}CD326^{neg}$ population containing, amongst others, mesenchymal cells. We found that nicotine induces a variety of strong effects immediately after birth that transiently increase the kinetics of lung development, and are then lost by pnd16. Finally, we also found that nicotine decreases the level of cell cycle of vascular endothelial cells at pnd8 and 16, thereby affecting one of the cell types involved in gas exchange. Even so the morphological changes do not seem to persist beyond pnd16, prenatal exposure to nicotine as well as to other compounds such as alcohol, stress, famine or toxicants contained in CS might result in a poor health outcome in adulthood. Indeed, epigenetic changes in different genes have been reported for nicotine. It will be important to understand whether this effect persists during the whole alveolar development phase and also later in life, and to address whether these subtle and transient changes detected at the beginning of alveolarization can leave a more permanent mark and affect lung health later in life.

ACKNOWLEDGEMENTS

We thank Eveline Yao for expert technical assistance and Stephan Tschanz for writing the software STEPanizer (www.stepanizer.com), the tool used for the stereological counting, and for helpful discussions. We also thank the Immunohistochemistry laboratory of the Pathology department, HUG, for their advices and help. We thank Genomic and Bioimaging core facilities of the Faculty of Medicine, University of Geneva, for their assistance and technical expertise. Finally, we thank Aliki Buhayer, Prism Scientific Sàrl (www.prismscientific.ch), for scientific and English writing support.

This work was supported by grants to Constance Barazzone-Argiroffo (Swiss National Science Foundation grant 310030-159500/1) and to Johannes Schittny (Swiss National Science Foundation grant 310030_175953), the Swiss Lung Liga and the Ligue pulmonaire Genevoise and the OPO-stiftung.

REFERENCES

1. **Barker DJ, and Osmond C**. Infant mortality, childhood nutrition, and ischaemic heart disease in England and Wales. *Lancet* 1: 1077-1081, 1986.

2. **Barletta KE, Cagnina RE, Wallace KL, Ramos SI, Mehrad B, and Linden J**. Leukocyte compartments in the mouse lung: distinguishing between marginated, interstitial, and alveolar cells in response to injury. *J Immunol Methods* 375: 100-110, 2012.

3. **Bultmann-Mellin I, Dinger K, Debuschewitz C, Loewe KMA, Melcher Y, Plum MTW, Appel S, Rappl G, Willenborg S, Schauss AC, Jungst C, Kruger M, Dressler S, Nakamura T, Wempe F, Alejandre Alcazar MA, and Sterner-Kock A**. Role of LTBP4 in alveolarization, angiogenesis, and fibrosis in lungs. *Am J Physiol Lung Cell Mol Physiol* 313: L687-L698, 2017.

4. **Cruz-Orive LM, and Weibel ER**. Sampling designs for stereology. *J Microsc* 122: 235-257, 1981.

5. **Cupul-Uicab LA, Skjaerven R, Haug K, Melve KK, Engel SM, and Longnecker MP**. In utero exposure to maternal tobacco smoke and subsequent obesity, hypertension, and gestational diabetes among women in the MoBa cohort. *Environ Health Perspect* 120: 355-360, 2012.

6. **Dai J, Wang Z, Xu W, Zhang M, Zhu Z, Zhao X, Zhang D, Nie D, Wang L, and Qiao Z**. Paternal nicotine exposure defines different behavior in subsequent generation via hyper-methylation of mmu-miR-15b. *Sci Rep* 7: 7286, 2017.

7. **Darzynkiewicz Z, Juan G, and Bedner E**. Determining cell cycle stages by flow cytometry. *Curr Protoc Cell Biol* Chapter 8: Unit 8 4, 2001.

8. **Dhalwani NN, Szatkowski L, Coleman T, Fiaschi L, and Tata LJ**. Nicotine replacement therapy in pregnancy and major congenital anomalies in offspring. *Pediatrics* 135: 859-867, 2015.

9. **Dobin A, Davis CA, Schlesinger F, Drenkow J, Zaleski C, Jha S, Batut P, Chaisson M, and Gingeras TR**. STAR: ultrafast universal RNA-seq aligner. *Bioinformatics* 29: 15-21, 2013.

10. **Drummond D, Baravalle-Einaudi M, Lezmi G, Vibhushan S, Franco-Montoya ML, Hadchouel A, Boczkowski J, and Delacourt C**. Combined Effects of in Utero and Adolescent Tobacco Smoke Exposure on Lung Function in C57Bl/6J Mice. *Environ Health Perspect* 125: 392-399, 2017.

11. **Epaud R, Aubey F, Xu J, Chaker Z, Clemessy M, Dautin A, Ahamed K, Bonora M, Hoyeau N, Flejou JF, Mailleux A, Clement A, Henrion-Caude A, and Holzenberger M**. Knockout of insulin-like growth factor-1 receptor impairs distal lung morphogenesis. *PLoS One* 7: e48071, 2012.

12. **Etzel RA**. A review of the use of saliva cotinine as a marker of tobacco smoke exposure. *Prev Med* 19: 190-197, 1990.

13. **Frank DB, Peng T, Zepp JA, Snitow M, Vincent TL, Penkala IJ, Cui Z, Herriges MJ, Morley MP, Zhou S, Lu MM, and Morrisey EE**. Emergence of a Wave of Wnt Signaling that Regulates Lung Alveologenesis by Controlling Epithelial Self-Renewal and Differentiation. *Cell Rep* 17: 2312-2325, 2016.

14. **Goniewicz ML, Eisner MD, Lazcano-Ponce E, Zielinska-Danch W, Koszowski B, Sobczak A, Havel C, Jacob P, and Benowitz NL**. Comparison of urine cotinine and the

549 tobacco-specific nitrosamine metabolite 4-(methylnitrosamino)-1-(3-pyridyl)-1-butanol (NNAL)
550 and their ratio to discriminate active from passive smoking. *Nicotine Tob Res* 13: 202-208, 2011.
551 15. **Gouveia L, Betsholtz C, and Andrae J**. PDGF-A signaling is required for secondary
552 alveolar septation and controls epithelial proliferation in the developing lung. *Development* 145:
553 2018.
554 16. **He JQ, Shumansky K, Connett JE, Anthonisen NR, Pare PD, and Sandford AJ**.
555 Association of genetic variations in the CSF2 and CSF3 genes with lung function in smoking-
556 induced COPD. *Eur Respir J* 32: 25-34, 2008.
557 17. **Huang LT, Chou HC, Lin CM, Yeh TF, and Chen CM**. Maternal nicotine exposure
558 exacerbates neonatal hyperoxia-induced lung fibrosis in rats. *Neonatology* 106: 94-101, 2014.
559 18. **Ievins R, Roberts SE, and Goldacre MJ**. Perinatal factors associated with subsequent
560 diabetes mellitus in the child: record linkage study. *Diabet Med* 24: 664-670, 2007.
561 19. **Kalina M, Mason RJ, and Shannon JM**. Surfactant Protein-C Is Expressed in Alveolar
562 Type-Ii Cells but Not in Clara Cells of Rat Lung. *American Journal of Respiratory Cell and*
563 *Molecular Biology* 6: 594-600, 1992.
564 20. **Kato T, Sato N, Takano A, Miyamoto M, Nishimura H, Tsuchiya E, Kondo S,**
565 **Nakamura Y, and Daigo Y**. Activation of placenta-specific transcription factor distal-less
566 homeobox 5 predicts clinical outcome in primary lung cancer patients. *Clin Cancer Res* 14:
567 2363-2370, 2008.
568 21. **Kent Pinkerton RH**. *The Lung, 2nd Edition*
569 *Development, Aging and the Environment*. 2014.

570 22. **Kinkead R, LeBlanc M, Gulemetova R, Lalancette-Hebert M, Lemieux M,**
571 **Mandeville I, and Jeannotte L**. Respiratory adaptations to lung morphological defects in adult
572 mice lacking Hoxa5 gene function. *Pediatr Res* 56: 553-562, 2004.
573 23. **Krick S, Grabner A, Baumlin N, Yanucil C, Helton S, Grosche A, Sailland J,**
574 **Geraghty P, Viera L, Russell DW, Wells JM, Xu X, Gaggar A, Barnes J, King GD, Campos**
575 **M, Faul C, and Salathe M**. Fibroblast growth factor 23 and Klotho contribute to airway
576 inflammation. *Eur Respir J* 52: 2018.
577 24. **Lauterstein DE, Tijerina PB, Corbett K, Oksuz BA, Shen SS, Gordon T, Klein CB,**
578 **and Zelikoff JT**. Frontal Cortex Transcriptome Analysis of Mice Exposed to Electronic
579 Cigarettes During Early Life Stages. *International Journal of Environmental Research and*
580 *Public Health* 13: 2016.
581 25. **Li Q, Gu Y, Tu Q, Wang K, Gu X, and Ren T**. Blockade of Interleukin-17 Restrains
582 the Development of Acute Lung Injury. *Scand J Immunol* 83: 203-211, 2016.
583 26. **Lillie RD**. *Histopathologic Technic and Practical Histochemistry*. New York: The
584 Blakiston Co., 1954.
585 27. **Mallakin A, Sugiyama T, Taneja P, Matise LA, Frazier DP, Choudhary M,**
586 **Hawkins GA, D'Agostino RB, Jr., Willingham MC, and Inoue K**. Mutually exclusive
587 inactivation of DMP1 and ARF/p53 in lung cancer. *Cancer Cell* 12: 381-394, 2007.
588 28. **Massaro D, and Massaro GD**. Critical period for alveologenesis and early determinants
589 of adult pulmonary disease. *Am J Physiol Lung Cell Mol Physiol* 287: L715-717, 2004.
590 29. **McFarlane L, Truong V, Palmer JS, and Wilhelm D**. Novel PCR assay for
591 determining the genetic sex of mice. *Sex Dev* 7: 207-211, 2013.

30. **McGowan SE, and McCoy DM**. Neuropilin-1 and platelet-derived growth factor receptors cooperatively regulate intermediate filaments and mesenchymal cell migration during alveolar septation. *Am J Physiol Lung Cell Mol Physiol* 315: L102-L115, 2018.

31. **Milger K, Holdt LM, Teupser D, Huber RM, Behr J, and Kneidinger N**. Identification of a novel SERPINA-1 mutation causing alpha-1 antitrypsin deficiency in a patient with severe bronchiectasis and pulmonary embolism. *Int J Chron Obstruct Pulmon Dis* 10: 891-897, 2015.

32. **Moffatt MF, Kabesch M, Liang L, Dixon AL, Strachan D, Heath S, Depner M, von Berg A, Bufe A, Rietschel E, Heinzmann A, Simma B, Frischer T, Willis-Owen SA, Wong KC, Illig T, Vogelberg C, Weiland SK, von Mutius E, Abecasis GR, Farrall M, Gut IG, Lathrop GM, and Cookson WO**. Genetic variants regulating ORMDL3 expression contribute to the risk of childhood asthma. *Nature* 448: 470-473, 2007.

33. **Mucenski ML, Wert SE, Nation JM, Loudy DE, Huelsken J, Birchmeier W, Morrisey EE, and Whitsett JA**. beta-Catenin is required for specification of proximal/distal cell fate during lung morphogenesis. *J Biol Chem* 278: 40231-40238, 2003.

34. **Mund SI, Stampanoni M, and Schittny JC**. Developmental alveolarization of the mouse lung. *Developmental Dynamics* 237: 2108-2116, 2008.

35. **Nabhan AN, Brownfield DG, Harbury PB, Krasnow MA, and Desai TJ**. Single-cell Wnt signaling niches maintain stemness of alveolar type 2 cells. *Science* 359: 1118-1123, 2018.

36. **National Cancer Institute (U.S.)**. NCI tobacco control monograph series. In: *NIH publication*. Bethesda, MD: U.S. Dept. of Health and Human Services, National Institutes of Health, National Cancer Institute, 2005, p. v.

614 37. **Nielsen S, King LS, Christensen BM, and Agre P**. Aquaporins in complex tissues. II.
615 Subcellular distribution in respiratory and glandular tissues of rat. *Am J Physiol* 273: C1549-
616 1561, 1997.
617 38. **Parent RA**. *Comparative biology of the normal lung*. Amsterdam: Elsevier/Academic
618 Press, 2015, p. xvii, 815 pages.
619 39. **Petre MA, Petrik J, Ellis R, Inman MD, Holloway AC, and Labiris NR**. Fetal and
620 neonatal exposure to nicotine disrupts postnatal lung development in rats: role of VEGF and its
621 receptors. *Int J Toxicol* 30: 244-252, 2011.
622 40. **Pozarska A, Rodriguez-Castillo JA, Surate Solaligue DE, Ntokou A, Rath P,**
623 **Mizikova I, Madurga A, Mayer K, Vadasz I, Herold S, Ahlbrecht K, Seeger W, and Morty**
624 **RE**. Stereological monitoring of mouse lung alveolarization from the early postnatal period to
625 adulthood. *Am J Physiol Lung Cell Mol Physiol* 312: L882-L895, 2017.
626 41. **Pusztaszeri MP, Seelentag W, and Bosman FT**. Immunohistochemical expression of
627 endothelial markers CD31, CD34, von Willebrand factor, and Fli-1 in normal human tissues.
628 *Journal of Histochemistry & Cytochemistry* 54: 385-395, 2006.
629 42. **Quinlan AR, and Hall IM**. BEDTools: a flexible suite of utilities for comparing
630 genomic features. *Bioinformatics* 26: 841-842, 2010.
631 43. **RDC T**. R: a language and environment for statistical computing. *R Foundation for*
632 *Statistical*
633 *Computing* 2011.
634 44. **Rehan VK, Asotra K, and Torday JS**. The effects of smoking on the developing lung:
635 insights from a biologic model for lung development, homeostasis, and repair. *Lung* 187: 281-
636 289, 2009.

637 45. **Ren K, Lv Y, Zhuo Y, Chen C, Shi H, Guo L, Yang G, Hou Y, Tan RX, and Li E**.
638 Suppression of IRG-1 Reduces Inflammatory Cell Infiltration and Lung Injury in Respiratory
639 Syncytial Virus Infection by Reducing Production of Reactive Oxygen Species. *J Virol* 90: 7313-
640 7322, 2016.
641 46. **Rennard SI, and Drummond MB**. Early chronic obstructive pulmonary disease:
642 definition, assessment, and prevention. *Lancet* 385: 1778-1788, 2015.
643 47. **Rennard SI, and Vestbo J**. COPD: the dangerous underestimate of 15%. *Lancet* 367:
644 1216-1219, 2006.
645 48. **Robinson MD, McCarthy DJ, and Smyth GK**. edgeR: a Bioconductor package for
646 differential expression analysis of digital gene expression data. *Bioinformatics* 26: 139-140,
647 2010.
648 49. **Roth-Kleiner M, Berger TM, Tarek MR, Burri PH, and Schittny JC**. Neonatal
649 dexamethasone induces premature microvascular maturation of the alveolar capillary network.
650 *Dev Dyn* 233: 1261-1271, 2005.
651 50. **Sakurai R, Cerny LM, Torday JS, and Rehan VK**. Mechanism for nicotine-induced
652 up-regulation of Wnt signaling in human alveolar interstitial fibroblasts. *Exp Lung Res* 37: 144-
653 154, 2011.
654 51. **Sandberg K, Poole SD, Hamdan A, Arbogast P, and Sundell HW**. Altered lung
655 development after prenatal nicotine exposure in young lambs. *Pediatr Res* 56: 432-439, 2004.
656 52. **Scherle W**. A simple method for volumetry of organs in quantitative stereology.
657 *Mikroskopie* 26: 57-60, 1970.
658 53. **Schittny JC**. Development of the lung. *Cell Tissue Res* 367: 427-444, 2017.

659 54. **Schittny JC, Mund SI, and Stampanoni M**. Evidence and structural mechanism for late
660 lung alveolarization. *Am J Physiol Lung Cell Mol Physiol* 294: L246-254, 2008.
661 55. **Sekhon HS, Jia Y, Raab R, Kuryatov A, Pankow JF, Whitsett JA, Lindstrom J, and**
662 **Spindel ER**. Prenatal nicotine increases pulmonary alpha7 nicotinic receptor expression and
663 alters fetal lung development in monkeys. *J Clin Invest* 103: 637-647, 1999.
664 56. **Silva JP, Lambert G, van Booven D, and Wahlestedt C**. Epigenomic and metabolic
665 responses of hypothalamic POMC neurons to gestational nicotine exposure in adult offspring.
666 *Genome Medicine* 8: 2016.
667 57. **Teo JL, and Kahn M**. The Wnt signaling pathway in cellular proliferation and
668 differentiation: A tale of two coactivators. *Adv Drug Deliv Rev* 62: 1149-1155, 2010.
669 58. **Wang NS, Chen MF, Schraufnagel DE, and Yao YT**. The cumulative scanning
670 electron microscopic changes in baby mouse lungs following prenatal and postnatal exposures to
671 nicotine. *J Pathol* 144: 89-100, 1984.
672 59. **Whittington JR, Simmons PM, Phillips AM, Gammill SK, Cen R, Magann EF, and**
673 **Cardenas VM**. The Use of Electronic Cigarettes in Pregnancy: A Review of the Literature.
674 *Obstet Gynecol Surv* 73: 544-549, 2018.
675 60. **Wongtrakool C, Wang N, Hyde DM, Roman J, and Spindel ER**. Prenatal nicotine
676 exposure alters lung function and airway geometry through alpha7 nicotinic receptors. *Am J*
677 *Respir Cell Mol Biol* 46: 695-702, 2012.
678 61. **Yan Z, Xiaoyu Z, Zhixin S, Di Q, Xinyu D, Jing X, Jing H, Wang D, Xi Z, Chunrong**
679 **Z, and Daoxin W**. Rapamycin attenuates acute lung injury induced by LPS through inhibition of
680 Th17 cell proliferation in mice. *Sci Rep* 6: 20156, 2016.

681 62. **Yang J, Hernandez BJ, Martinez Alanis D, Narvaez del Pilar O, Vila-Ellis L,**
682 **Akiyama H, Evans SE, Ostrin EJ, and Chen J**. The development and plasticity of alveolar
683 type 1 cells. *Development* 143: 54-65, 2016.
684 63. **Zanetti F, Giacomello M, Donati Y, Carnesecchi S, Frieden M, and Barazzone-**
685 **Argiroffo C**. Nicotine mediates oxidative stress and apoptosis through cross talk between NOX1
686 and Bcl-2 in lung epithelial cells. *Free Radic Biol Med* 76: 173-184, 2014.
687 64. **Zou W, Liu S, Hu J, Sheng Q, He F, Li B, and Ran P**. Nicotine reduces the levels of
688 surfactant proteins A and D via Wnt/beta-catenin and PKC signaling in human airway epithelial
689 cells. *Respir Physiol Neurobiol* 221: 1-10, 2016.
690 65. **Zou W, Zou Y, Zhao Z, Li B, and Ran P**. Nicotine-induced epithelial-mesenchymal
691 transition via Wnt/beta-catenin signaling in human airway epithelial cells. *Am J Physiol Lung*
692 *Cell Mol Physiol* 304: L199-209, 2013.
693

694 **FIGURE LEGENDS**

695 Figure 1. Morphology and stereological analysis of pup lungs. Stereological analysis
696 was performed on H&E lung sections of post-natal day (pnd) 2, 8 and 16 from control
697 and nicotine group (A). lung volume (B), parenchyma volume (C), septal volume (D),
698 septal surface area (E) and mean linear intercept (MLI, F) were measured at pnd2, 8
699 and 16. Control/Nicotine group; For pnd2 and 16 n=5 animals was used for each
700 group (for pnd2, 2 females (F), 2 males (M) and one not determined in the control
701 group and 3M and 2F in the nicotine group; for pnd16, 5M in the control group and
702 3F and 2M in the nicotine group), for pnd8 n=3 animals for each group (2F and 1M in
703 the control group and 1F and 2M in the nicotine group). Results are presented as
704 individual plots and mean values ±SD. * $p<0.05$; *n.s.* not significant. The comparison
705 was done between control and nicotine group for each time point with two way
706 ANOVA and Bonferroni correction.
707

708 Figure 2. Comparison of RNAseq analysis of lung extracts of control and nicotine
709 exposed mice. Analysis of RNAseq data, was done at pnd2 (n=6 animals for control
710 group (4F and 2M) and n=5 animals for nicotine group (3F and 2M)) and pnd16 (n=5
711 animals for control group (2F and 3M) and n=3 animals for nicotine group(2F and
712 1M)) and is represented as a two-dimensional MDS plot with samples in red for the
713 control group and in purple for the nicotine group (A). Pathway analysis performed at
714 pnd2 with MetaCore software (with threshold of two and significance $p<0.05$) is
715 shown in (B) for nicotine-induced pathways and in (C) for nicotine-downregulated
716 pathways.

Figure 3. Nicotine upregulates canonical WNT/β-catenin signaling pathway. Lung tissues were processed at pnd2, 8 and 16 from control and nicotine group and analyzed by immunohistochemistry (A and B) and western blot (C and D). To address cell proliferation we measured Ki67 expression (A, n=4-11 animals/pnd/condition) and for apoptosis we used TUNEL staining (B, n=4-8 animals/pnd/condition). WNT pathway was accessed by measuring the expression of β-catenin (C, n=3 animals/pnd/condition) and survivin (D, n=3 animals/pnd/condition). Actin was used as a loading control in western blot analysis (C and D).* significance for nicotine treatment *vs.* control between different pnds. #significance pnd16/8 vs pnd2; † significance pnd16 vs pnd8; $^{\#\#\#\#/\dagger\dagger\dagger\dagger}$ $p<0.0001$; *n.s,* not significant (A and B). The average of sepaate western blot experiments is shown. $p<0.05$; *n.s,* not significant. T-test analysis was performed between control and nicotine group for each time point (C and D).

Figure 4. Nicotine affects cell cycling of vascular endothelial cells and AEC type I. Cells were isolated from mouse lung at pnd2, 8 and 16 and percent of cycling cells was determined by Hoechst staining via FACS in different cell populations: vascular endothelial cells ($CD31^{pos}$) (A), mature AEC type II cells ($CD326^{pos}MHCII^{pos}$) (B), AEC type I cells ($CD326^{pos}PDPN^{high}$) (C) and mesenchymal cells ($CD31^{neg}CD326^{neg}$) (D). n = 5-10 animals/condition and pnd were used for the analysis. Graphical representation of the data are shown; * significance for nicotine treatment *vs.* control between different pnds. #significance pnd16/8 vs pnd2; † significance pnd16 vs pnd8; $^{*/\#}$ $p<0.05$; $^{\#\#/\dagger\dagger}$ $p<0.01$; $^{\#\#\#\#/\dagger\dagger\dagger\dagger}$ $p<0.0001$; *n.s.* not significant.

741 Figure 5. IHC of alveolar cells in nicotine–exposed and non-exposed pups. Lung
742 paraffin sections of the control and nicotine–exposed pups from pnd2, 8 and 16 were
743 stained with IgG antibody control (upper panel) and AEC type II marker (SPC)
744 (middle and lower panel)(A). Graphical quantification for this marker is also shown in
745 (A). SPC positive cells at pnd2 and 16 are indicated with red arrows. Analysis was
746 performed on 10 different fields/lung (dimensions 210μm x 110μm) and 3-5
747 animals/group. Results are presented as total number of positive cells per cm^2 of lung
748 tissue. * significance for nicotine treatment *vs.* control between different pnds.
749 #significance pnd16/8 vs pnd2; † significance pnd16 vs pnd8; $^{*/\#}$ $p<0.05$; $^{\#\#/\dagger\dagger}$ $p<0.01$;
750 $^{\#\#\#}$ $p<0.001$; *n.s.* not significant. Lung cryosections of the control pups from pnd2 and
751 16, stained for AEC type I marker PDPN and the marker of vascular endothelial cells,
752 CD31, are shown in (B). The first column represents staining with IgG control, and
753 the middle and last column show staining with the corresponding antibodies.
754
755 Figure 6. FACS isolation of alveolar cells during lung development in nicotine-
756 exposed and non-exposed pups. Cells were isolated from mouse lung at pnd2, 8 and
757 16 and sorted by FACS based on expression of CD45 marker. $CD45^{neg}$ population (A)
758 was further analyzed for the expression of following markers: mesenchymal cells
759 ($CD31^{neg}CD326^{neg}$) (B), $CD31^{pos}PDPN^{neg}$ (vascular endothelial cells) (C),
760 $CD326^{pos}PDPN^{high}$ (AEC type I cells) (D) and $CD326^{pos}MHCII^{pos}$ (mature AEC type
761 II cells) (E). n = 5-10 animals/condition and pnd were used for the analysis. Graphical
762 representation of the data are shown; * significance for nicotine treatment *vs.* control
763 between different pnds. #significance pnd16/8 vs pnd2; † significance pnd16 vs pnd8;
764 $^{*/\#}$ $p<0.05$; $^{\#\#\#}$ $p<0.001$; $^{****/\#\#\#\#/\dagger\dagger\dagger\dagger}$ $p<0.0001$; *n.s.* not significant.
765

766 **SUPPLEMENTAL MATERIAL**

767 The supplemental material (Figures S1 to S4 and the list of antibodies and reagents) is

768 deposited in a generalist public access repository figshare

769 (https://figshare.com/s/56282a06102729a7ee90) (DOI:10.6084/m9.figshare.8201696).

770

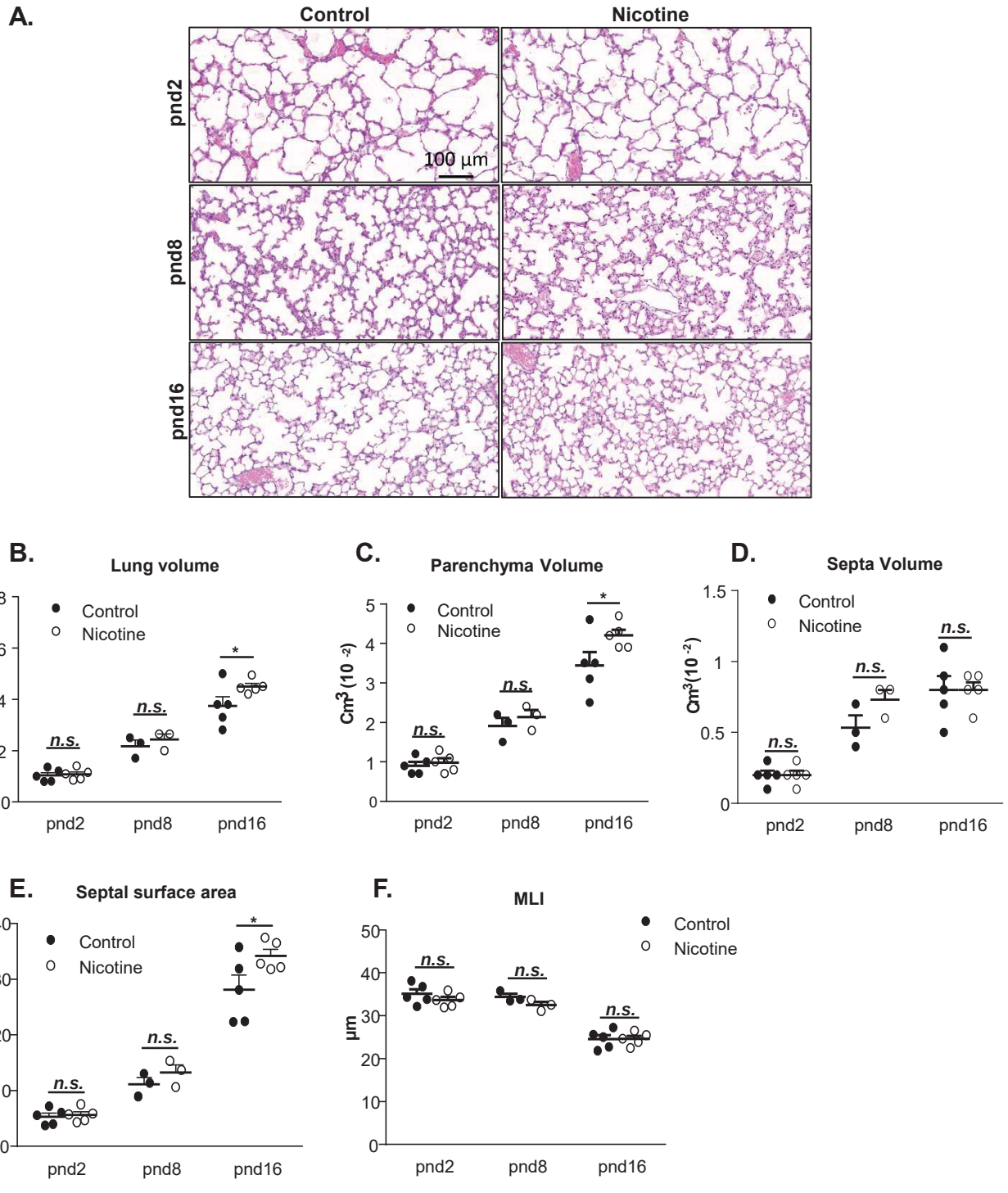

Blaskovic et al. Figure 2.

A.

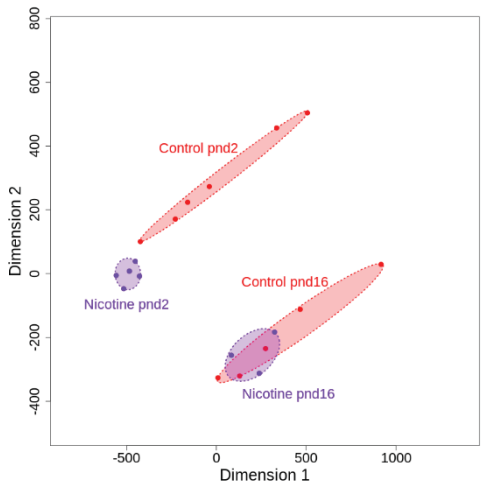

B.

Cell cycle (the metaphase checkpoint)
Cell cycle (APC in cell cycle regulation)
Cell cycle (chromosome condensation)
Development (EMT)
Stem cells (myogenesis)
Canonical WNT
WNT (inhibition of oligodendrocyte precursor cell differentiation)
Stromal-epithelial interaction in prostate cancer
Cell adhesion and ECM remodeling
DNA damage (ATM/ATR regulation of G1/S checkpoint)

C.

Immune response (IL10 signaling)
Immune response (IL6 signaling)
TNFalpha inflammatory signaling in airway epithelium
Vascular endothelial cell damage
Immune response (HSP60/70 and TLR signaling)
Cytokines in asthma (neutrophil-derived)
Immune response (IL17 signaling)
Immune response (IL1 signaling)
Neutrophil chemotaxis in asthma
Release of pro-inflammatory factors by alveolar macrophages (asthma)

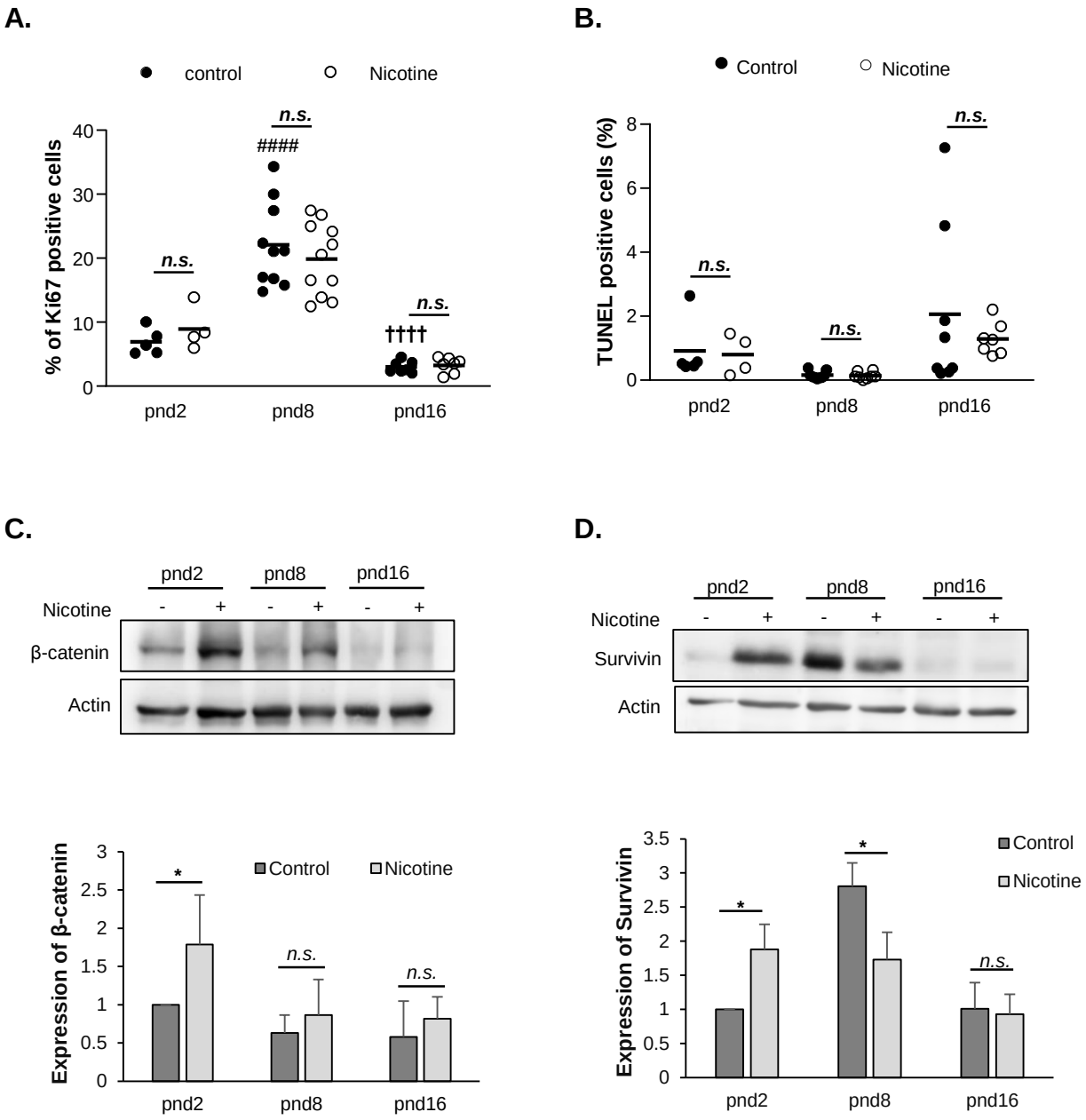

Blaskovic et al. Figure 4.

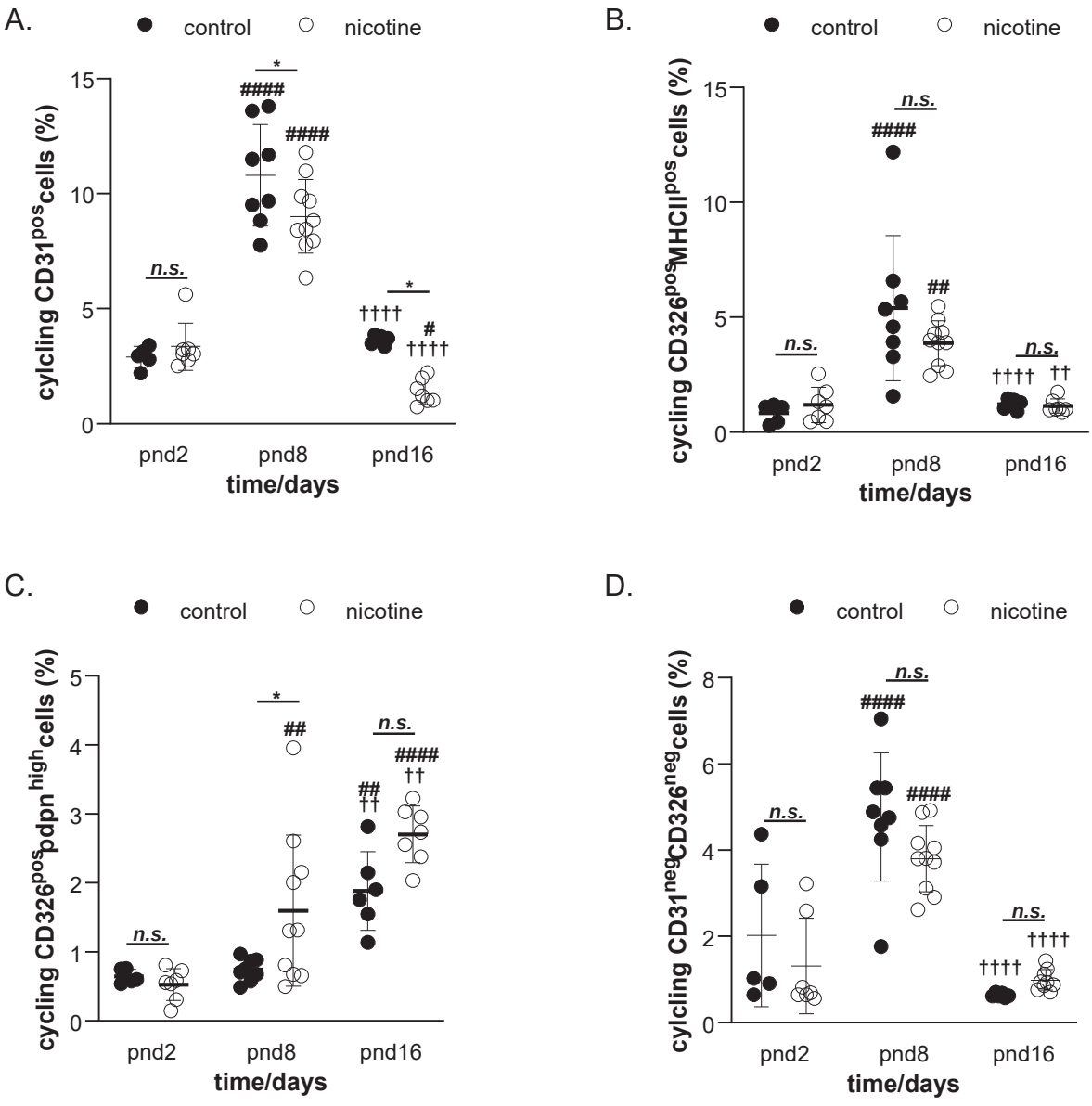

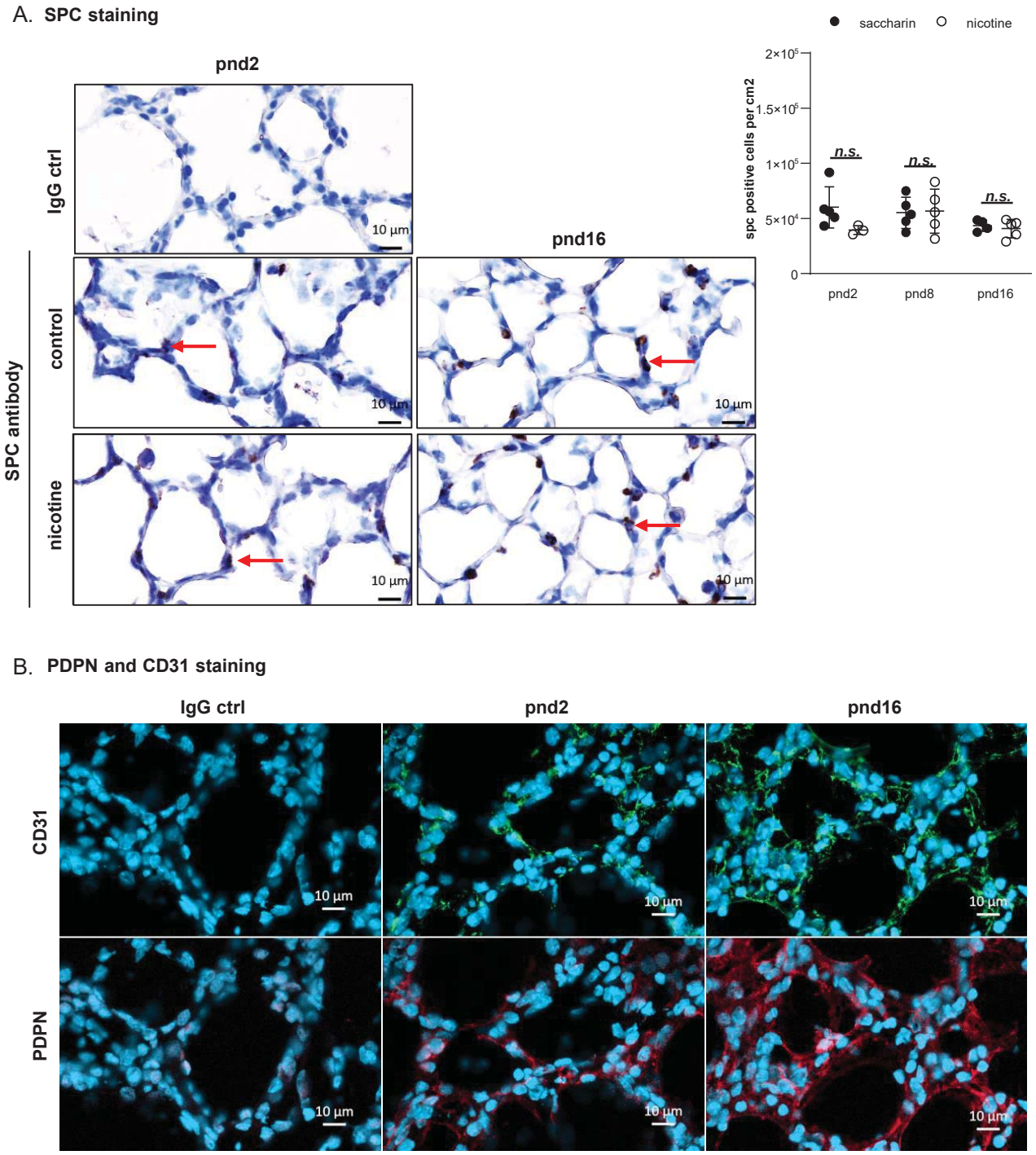

Blaskovic et al. Figure 6.

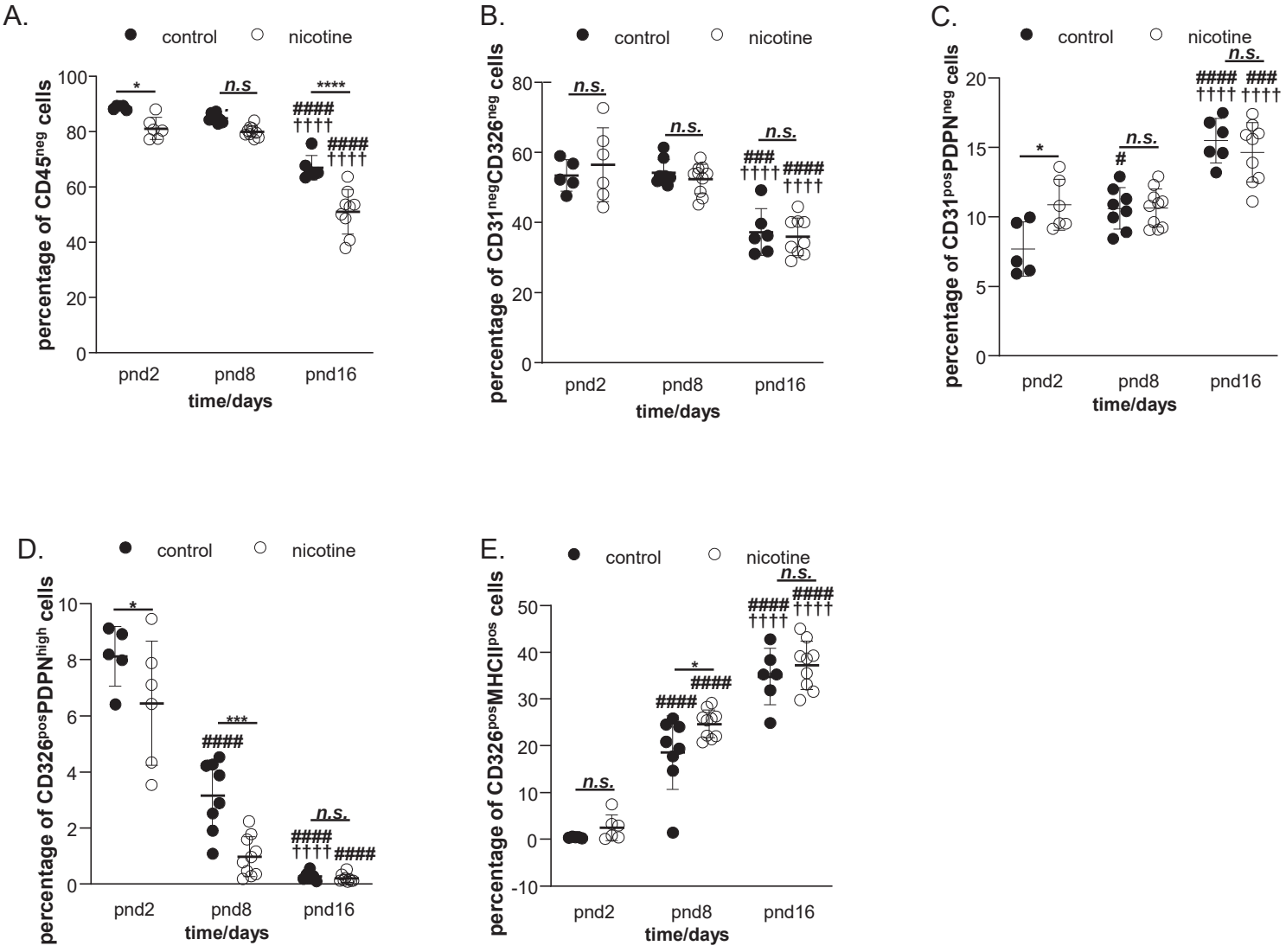

TABLES

Table 1. Lung morphometry of mouse lungs analyzed from pnd2 to pnd16

	control					
Morphometry	pnd2 (n=5)	pnd8 (n=3)	pnd16 (n=5)	p^a	P^b	P^c
Lung volume (cm^3)	0.01 ± 0.002	0.022 ± 0.004	0.04 ± 0.008	0.0513	**<0.0001**	**0.0092**
Parenchyma volume (cm^3)	0.009 ± 0.002	0.019 ± 0.004	0.03 ± 0.008	0.0638	**<0.0001**	**0.0066**
Septa volume (cm^3)	0.002 ± 0.001	0.005 ± 0.001	0.008 ± 0.002	**0.0458**	**0.0005**	0.1128
Septal surface area (cm^2)	5.3 ± 1.4	11.2 ± 2.1	28.15 ± 5.9	0.1566	**<0.0001**	**0.0004**
Mean linear intercept (μm)	35.1 ± 2.4	34.4 ± 1.2	24.5 ± 2.2	0.8916	**<0.0001**	**0.0002**

pnd = post-natal day;

Mean values ± SD are reported.

P Pairwise statistical comparison one-way ANOVA with tukey correction was performed between day 2 and 8 (P^a), day 2 and 16 (P^b), and day 8 and 16 (P^c)

Values reported are for lung right middle lobe.

Table 2. Top 10 of UP- and DOWN-regulated genes upon nicotine *in utero* exposure at pnd2

Symbol	Gene name	Function	Lung-related function	FC
Bglap	Osteocalcin	Bonne remodeling/energy metabolism	N/A	316
Mepe	Matrix Extracellular Phosphoglycoprotein	Bone ECM	N/A	274
Bglap2	Bone Gamma-Carboxyglutamate Protein 2	Bonne remodeling/energy metabolism	N/A	180
Dlx5	Distal-Less Homeobox 5	Osteoblast differentiation	Oncogene in lung cancer	175
Dmp1	Cyclin D binding myb-like protein 1	P53 pathway regulator	Lung cancer	124
Myoz3	Myozenin 3	Regulator of calcineurin	N/A	119
Atp1b4	ATPase Na+/K+ Transporting Family Member Beta 4	Regulation of active transport	N/A	81
Ostn	Osteocrin	Glucose metabolism in skeletal muscle/osteoblasts differentiation	N/A	80.5
Myh2	Myosine heavy chain	Muscle contraction	pneumonia	64
Ctrnd	Cholinergic receptor Nicotinic Delta Subunit	Acetylcholine/nicotine receptor	Lung cancer	63
Fgf23	Fibroblast growth factor 23	Phosphate and vitamine D metabolism	Fgf-23−/− mouse exhibit premature aging and lung emphysema	-606.5
Csf3	Granulocyte colony stimulating factor 3	production, differentiation, and function of granulocytes	Lung metastasis ;	-219
8030474K03Rik		N/A	N/A	-196
Il22	Interleukin 22	Innate and adaptive immune response	Lung epithelial repair after injury	-178.5
Cxcl2	C-X-C Motif Chemokine Ligand 2	Angiogenic chemokine	Regulation of airway smooth muscle cell migration	-148.4
Irg1	Aconitate Decarboxylase 1	Inhibitor of toll-like receptor-mediated inflammatory response	Suppression improves immune lung injury after RSV infection by reducing ROS production	-132
Il17f	Interleukin17f	Innate and adaptive immune response	Protection from bacteri/fungi and involved in repair	-129
Orm2	Orosomucoid 2	modulating immunity, maintaining the barrier function of capillary, sphingolipid metabolism	asthma	-96
Orm3	Orosomucoid 3	modulating immunity, maintaining the barrier function of capillary, sphingolipid metabolism	asthma	-92
Orm1	Orosomucoid 1	modulating immunity, maintaining the barrier function of capillary, sphingolipid metabolism	asthma	-90

FC = fold change

Table 3. Relative abundance of alveolar cells analyzed by FACS during lung development from pnd2 to pnd16

	control						
Cell type %	pnd2 (n=5)	pnd8 (n=8)	pnd16 (n=6)	p^a	P^b	P^c	F(DFn, Dfd)
$CD45^{neg}$	88.8 ± 0.8	84.9 ± 1.5	67 ± 4.5	0.1362	**0.0004**	**0.0006**	104(2,4)
$CD45^{neg}CD31^{neg}CD326^{neg}$	53.4 ± 4.5	54.25 ± 3.7	37.3 ± 6.6	0.9898	**0.0300**	**0.0194**	13.2(2,4)
EC ($CD31^{pos}PDPN^{neg}$)	7.7 ± 1.9	10.6 ± 1.5	15.5 ± 1.6	0.0788	**0.0034**	**0.0125**	31(2,4)
AEC type I($CD326^{pos}PDPN^{high}$)	8.1 ± 1.1	3.2 ± 1.3	0.3 ± 0.2	**0.0049**	**0.0011**	**0.0271**	54.3(2,4)
AEC type II($CD326^{pos}MHCII^{pos}$)	0.4 ± 0.1	18.55 ± 7.9	34.8 ± 6.1	0.0659	**0.0082**	0.0584	18.4(2,4)

Percentages of endothelial and epithelial populations are expressed as mean ± SD after exclusions of $CD45^{pos}$ population.

Nested one-way ANOVA was performed to determine statistical significance.

P Pairwise statistical comparison one-way ANOVA with Turkey correction was performed between day 2 and 8 (P^a), day 2 and 16 (P^b), and day 8 and 16 (P^c); degrees of freedom are reported with degrees of freedom numerator (DFn) and denominator (DFd) values.

pnd = post-natal day; EC = endothelial cells; PDPN = podoplanin; MHCII = major histocompatibility complex class II